JOURNAL OF THERMOPHYSICS AND HEAT TRANSFER
Vol. 13, No. 4, October–December 1999

Mixed-Convection Heat Transfer in Concave and Convex Channels

F. Moukalled* and A. Doughan†
American University of Beirut, Beirut, Lebanon
and
S. Acharya‡
Louisiana State University, Baton Rouge, Louisiana 70803-6413

A numerical investigation of laminar mixed-convection heat transfer of air in concave and convex channels is presented. Six different channel aspects ratios (R/L = 1.04, 1.25, 2.5, 5, 10, and ∞) and five different values of Gr/Re^2 (Gr/Re^2 = 0, 0.1, 1, 3, 5) are considered: results are displayed in terms of streamline and isotherm plots, velocity and temperature profiles, and local and average Nusselt number estimates. Numerical predictions reveal that compared to straight channels of equal height concave channels of low aspect ratio have lower heat transfer at relatively low values of Gr/Re^2 and higher heat transfer at high values of Gr/Re^2. When compared to straight channels of equal heated length, concave channels are always found to have lower heat transfer and for all values of Gr/Re^2. On the other hand, predictions for convex channels revealed enhancement in heat transfer compared to straight channels of equal height and/or equal heated length for all values of Gr/Re^2.

Nomenclature

c_p	= specific heat
Gr_L	= Grashof number, $g\beta\rho_0^2(T_w - T_0)L^3/\mu^2$
g	= gravitational acceleration
H	= height of the hot wall
k	= fluid thermal conductivity
L	= channel inlet width
$\overline{Nu}$	= average Nusselt number
Nu_S	= local Nusselt number
P	= dimensionless pressure
Pe	= Peclet number, $Re_L Pr$
Pr	= Prandtl number, $\mu c_P/k$
p	= dimensional pressure
R	= radius of curvature
Re_L	= Reynolds number, $\rho_0 v_0 L/\mu$
S	= dimensionless length of hot wall
T	= dimensional temperature
T_W	= dimensional wall temperature
T_0	= dimensional inlet temperature
U, V	= dimensionless velocity components
u, v	= dimensional velocity components
v_0	= mean inlet velocity
X, Y	= dimensionless coordinates
x, y	= dimensional coordinates
β	= thermal expansion coefficient
θ	= dimensionless temperature
μ	= dynamic viscosity
ξ, η	= boundary-fitted curvilinear coordinates
ρ, ρ_0	= density and reference density

Introduction

MIXED-CONVECTION heat-transfer studies in the literature have been primarily confined to pipe and rectangular channel geometries. In some applications, however, heat transfer in curved channels may be of interest (e.g., nozzle- and diffuser-shaped passages in heating, ventilation, and air conditioning systems, fume hoods, chimneys, bell-shaped or dome-shaped chemical reactors, etc.). In other applications, such as energy conservation in buildings, studies typically have not been made to determine the shape that optimizes heat transfer. For a given height, curved surfaces provide a larger area for heat transfer compared to straight surfaces. Therefore, in channels having curved walls, buoyancy may significantly augment heat transfer compared to straight channels of equal height. However, because of changes in the flow cross-sectional area associated with the curved surface, pressure gradient (favorable or adverse) can aid or oppose the buoyancy-induced acceleration. Mixed convection in channels with curved-entry surfaces has not been seriously investigated and represents the focus of the present investigation. The geometry selected in this paper is a generic configuration of a concave or convex surface bounded by an adiabatic wall. This study aims to explore the combined effects of pressure gradient and buoyancy on the surface heat transfer.

Several investigations have dealt with mixed-convection heat transfer in straight channels and pipes. Ostrach[1] studied fully developed laminar mixed convection of fluids in straight channels with linearly varying wall temperatures. Tao[2] examined analytically the fully developed mixed-convection flow in rectangular channels and between two vertical parallel plates with constant axial heat flux. Lawrence and Chato[3] used a numerical method for the calculation of developing flows between vertical plates with either constant wall heat flux or constant wall temperature. Zeldin and Schmidt[4] investigated numerically and experimentally developing mixed-convection flows in vertical tubes. Habchi and Acharya[5] presented numerical results for laminar mixed-convection heat transfer in symmetrically or asymmetrically heated vertical channels.

A number of studies have also considered mixed convection in more complex flow configurations. Hong et al.[6] considered mixed convection past a two-dimensional backstep and examined the effects of inclination angle and Prandtl number. Abu-Mulaweh et al.[7] investigated experimentally laminar mixed convection behind a two-dimensional backward-facing step for the buoyancy-opposing case. Thereafter, Abu-Mulaweh et al.[8] reported measurements of buoyancy-assisting, laminar mixed-convection flow of air along a two-dimensional, vertical backward-facing step. Habchi and Acharya[9] reported on laminar mixed-convection heat transfer in a partially blocked, vertical channel. Moukalled and Acharya[10] and

Received 28 July 1998; revision received 24 May 1999; accepted for publication 28 May 1999.

*Professor, Mechanical Engineering Department, Faculty of Engineering and Architecture.
†Graduate Student, Mechanical Engineering Department, Faculty of Engineering and Architecture.
‡Professor, Mechanical Engineering Department.

Moukalled et al.[11–13] investigated numerically laminar forced and mixed-convection heat transfer in externally finned pipes and examined the influence of pipe thermal conductivity on heat transfer. Moukalled et al.[11] extended the work reported in Moukalled and Acharya[10] to turbulent flow situations. Agonafer and Watkins[14] studied natural-convection heat transfer between diverging isothermal plates.

Work has also been reported on forced convection past curved surfaces. This body of work has been performed primarily in relation to external heat transfer over turbine blades. Concave curvature is known to destabilize laminar boundary layers that can lead to three-dimensional effects. Kestoras and Simon[15] and Finnis and Brown[16] provide a perspective on work reported in this area. However, no work on curved surfaces has been reported where buoyancy effects have also been included.

From the preceding literature survey, one can see that convection heat transfer over curved surfaces has not been given considerable attention. The objective of this study is to bridge this gap and to analyze the heat-transfer characteristics of laminar mixed-convection heat transfer in concave and convex channels.

Governing Equations

The physical situation under consideration is illustrated schematically in Fig. 1a. The left wall of the channel is vertical, whereas the right wall is curved and constitutes a part of a circle of radius R. Depending on whether the center of the circle is to the right or to the left of the curved surface (Fig. 1a), a concave or convex channel is obtained, respectively. In the concave channel the flow cross-sectional area increases in the flow direction, and an adverse pressure gradient is experienced by the flow. In the convex channel the flow cross-sectional area decreases in the flow direction, and a favorable pressure gradient is experienced by the flow. Note that the terms concave and convex reflect the curvature seen by an observer positioned outside the channel. The flow itself (and an observer inside the channel) will experience the opposite curvature.

The thermal boundary condition considered is asymmetric heating where the curved wall is maintained at a uniform temperature T_W and the vertical wall is insulated. The working fluid, taken to be air, enters the channel from the bottom with a parabolic-velocity profile and a uniform temperature T_0 ($T_0 < T_W$).

The equations governing the flow and temperature fields are those expressing the conservation of mass, momentum, and energy. The two-dimensional flow is considered to be steady, laminar, and of constant thermal properties except for density. Moreover, variations in density are assumed to be small except when appearing in the body force term of the y-momentum equation where they are expressed using the Boussinesq approximation.

The following dimensionless parameters are introduced to nondimensionalize the equations:

$$X = \frac{x}{L}, \qquad Y = \frac{y}{L}, \qquad U = \frac{u}{v_0}, \qquad V = \frac{v}{v_0}$$

$$\theta = \frac{T - T_0}{T_w - T_0}, \qquad P = \frac{p + \rho_0 g y}{\rho_0 v_0^2} \tag{1}$$

where v_0 is a reference velocity equal to the mean velocity of the flow at the inlet/exit to the concave/convex channel. The governing differential equations in nondimensional forms can be written as

$$\frac{\partial U}{\partial X} + \frac{\partial V}{\partial Y} = 0 \tag{2}$$

$$U\frac{\partial U}{\partial X} + V\frac{\partial U}{\partial Y} = -\frac{\partial P}{\partial X} + \frac{1}{Re_L}\left(\frac{\partial^2 U}{\partial X^2} + \frac{\partial^2 U}{\partial Y^2}\right) \tag{3}$$

$$U\frac{\partial V}{\partial X} + V\frac{\partial V}{\partial Y} = -\frac{\partial P}{\partial Y} + \frac{1}{Re_L}\left(\frac{\partial^2 V}{\partial X^2} + \frac{\partial^2 V}{\partial Y^2}\right) + \frac{Gr_L}{Re_L^2}\theta \tag{4}$$

$$U\frac{\partial \theta}{\partial X} + V\frac{\partial \theta}{\partial Y} = \frac{1}{Pe}\left(\frac{\partial^2 \theta}{\partial X^2} + \frac{\partial^2 \theta}{\partial Y^2}\right) \tag{5}$$

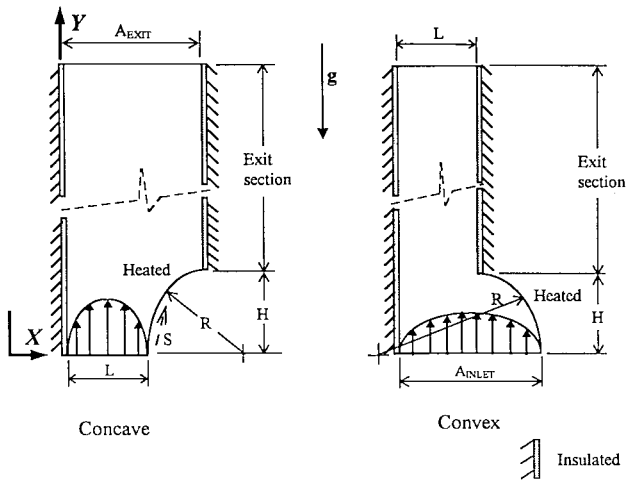

Fig. 1a Schematic of concave and convex channels.

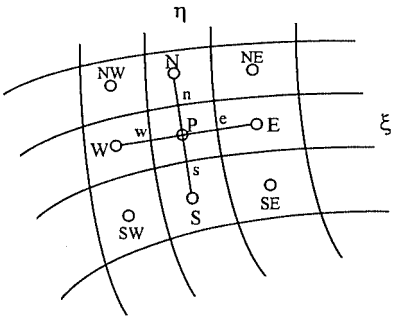

Fig. 1b Typical control volume.

The boundary conditions used are as follows.

At inlet:

$$V = 6(X - X^2), \qquad U = \theta = 0 \tag{6}$$

Along the heated wall:

$$U = V = 0, \qquad \theta = 1 \tag{7}$$

Along the insulated walls:

$$U = V = \frac{\partial \theta}{\partial X} = 0 \tag{8}$$

At the exit:

$$\frac{\partial U}{\partial Y} = \frac{\partial V}{\partial Y} = \frac{\partial \theta}{\partial Y} = 0 \tag{9}$$

The exit section of the channel is made long enough (as shown in Fig. 1) to safely apply the outflow boundary condition. For the concave channel, where flow separation occurs, it was necessary to make the length of the exit chimney section to be 33 times the height of the concave section. For the convex channel, where no flow separation is obtained, the exit section is only three times the height of the convex surface.

Solution Procedure

The coupled system of equations governing the flow and temperature fields [Eqs. (2–5)] is solved numerically using the control volume approach. In this method the solution domain is divided into a number of control volumes, each associated with a main grid point P (Fig. 1b). The discretized form is obtained by first expressing Eqs. (2–5) using a general curvilinear coordinate system (ξ, η) and then integrating the resulting equations over the control volume shown in Fig. 1b. The integrated equations are reduced into algebraic equations by expressing the variation in the dependent variable and its derivatives in terms of the grid point values using the power law scheme of Patankar,[17] and the resulting system of algebraic

equations is solved by a line-by-line Thomas algorithm.[17] The unknown pressure field is obtained using the SIMPLE algorithm of Patankar.[17] Moreover, solutions are obtained over a nonstaggered grid in which checkerboard pressure and velocity fields are eliminated through the use of the pressure weighted interpolation method (PWIM) of Peric.[18] All computations are performed using nonuniform grids with denser clustering near the walls where boundary layers develop and high gradients are expected. Grid networks are generated using the transfinite interpolation technique.[19]

To investigate the sensitivity of the solution to the grid used, numerical experiments were carried out in convex channels on three different sizes of nonuniform grids of density: 21×51, 31×81, and 51×101. The computed average Nusselt number values for $R/L = 1.25$ are shown in Table 1. As depicted, the maximum difference in these values between the 31×81 and 51×101 grids is less than 0.43%. The velocity and temperature profiles on the three different grid sizes are shown in Fig. 2 at two streamwise locations ($Y = 0.5$ and 0.9). The solutions are very close to each other, with the 31×81 grid solution and the 51×101 grid solution showing virtually identical results. Therefore, as a compromise between smoothness and CPU time, the 31×81 grid system is used for all calculations in convex channels.

Similar tests with three different grid sizes (21×51, 31×231, and 51×281) were conducted to determine the size of the grid needed to obtain grid-independent solutions in concave channels. The grid independence is demonstrated by the velocity and temperature solutions on the three grid sizes shown in Fig. 2. Again, all three solutions are very close to each other. A 31×231 grid was found to be adequate and was used for all computations. The significantly greater number of grid points needed in the flow direction are because of the longer exit section associated with the concave channel.

Table 1 Grid size tests for concave channel

	Average Nusselt number			
Grid size	21×51	31×81	51×101	Maximum difference, %
$Gr/Re^2 = 0.1$	9.46	9.31	9.35	0.43
$Gr/Re^2 = 1.0$	9.77	9.69	9.71	0.21
$Gr/Re^2 = 3.0$	10.53	10.42	10.44	0.19
$Gr/Re^2 = 5.0$	11.08	11.02	10.99	0.29

As a further check for accuracy, the velocity profile across a vertically oriented, asymmetrically heated straight channel computed by Habchi and Acharya[9] is compared against the profile obtained by the present code using the same flow parameters (Fig. 3). The two sets of results compare very well and are nearly identical, confirming the credibility of the solution procedure and algorithm used.

Finally, results for the concave channel were compared with the mixed convection experiments past a backstep reported by Abu-Mulaweh et al.[8] Although the backstep geometry exhibits some of the features of the flow in a concave channel (i.e., flow expansion, adverse pressure gradient), there are differences in the length of the recirculation regions and flow patterns, and therefore a good agreement between the two solutions is not expected. However, it is anticipated that as the flow recovers past the separation the results of the two problems will approach each other. With this in mind, a specific case from Ref. 8 was selected ($u_\infty = 0.41$ m/s, $\Delta T = 10°$C, stepheight = 0.8 cm, $Gr/Re^2 = 0.016$), and results were obtained for an analogous concave channel with the same expansion ratio ($R/L \sim 41.5$), Re, and Gr values. Also the same thermal boundary conditions (constant wall temperature) as in Ref. 8 were employed. The Nusselt number along the heated wall (downstream of the step or curved surface) and the velocity and temperature distributions at three different streamwise locations (again measured downstream of the step) are shown in Figs. 3b–3e. In the experiments the flow reattachment occurs in the vicinity of $Y = 6$, and significant differences in the backstep and concave channel results are observed upstream of this location. This is expected because for $R/L \sim 41.5$ there is no flow recirculation associated with the concave channel. As can be seen from the velocity profile at $Y = 2.5$, the backstep shows significant negative velocities, whereas for the concave channel no negative velocities are noted. However, beyond $Y = 6$, the backstep measurements and the concave channel predictions approach each other, and at $Y = 18.75$ the measured and predicted profiles are identical to each other (Figs. 3b and 3e). The excellent agreement between measurements and predictions following the separation

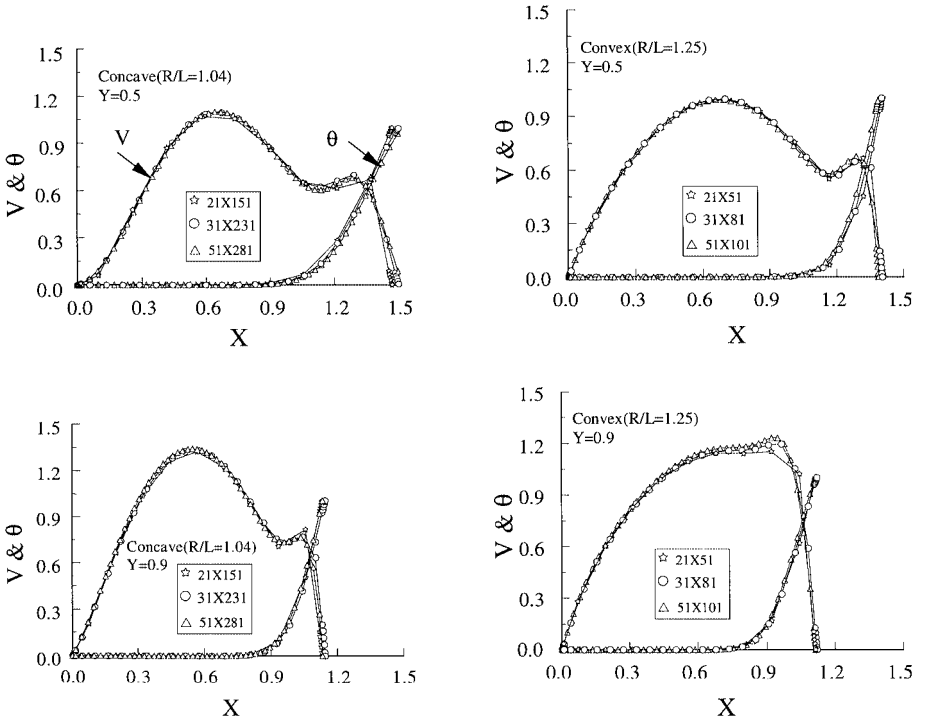

Fig. 2 Effects of mesh sizes on velocity and temperature profiles in concave and convex channels.

region again points to the validity of the numerical scheme and the grid used.

Results and Discussion

The parameters affecting heat transfer in this study are the aspect ratio R/L, the Grashof number Gr, the Reynolds number Re, and the Prandtl number Pr. Parameter values considered are six different channel aspect or curvature ratios ($R/L = 1.04, 1.25, 2.5, 5, 10$, and ∞) and five different values of Gr/Re^2 ($Gr/Re^2 = 0$, 0.1, 1, 3, and 5). A curvature ratio of ∞ represents a vertical flat channel. The value of Re is fixed at 100 to represent laminar flow. Air ($Pr = 0.72$) is chosen as the working fluid, and, therefore, Pe is fixed at 72.

To reveal the effects of the various parameters on heat transfer, results are presented in terms of streamline and isotherm plots, velocity and temperature profiles, and local and average Nusselt-number values. The streamline and isotherm plots are presented only for a limited vertical region of interest (and do not extend all the way to the channel exit) to preserve clarity of the figures.

Concave Channels

The concave-channel configuration corresponds to the case where buoyancy and adverse pressure gradient (associated with flow expansion) oppose each other, and thus produce counteracting effects on the surface heat transfer. Thus, depending on the surface curvature, and Re and Gr/Re^2 values, both enhancement and degradation of overall heat transfer is possible relative to the vertical channel configuration.

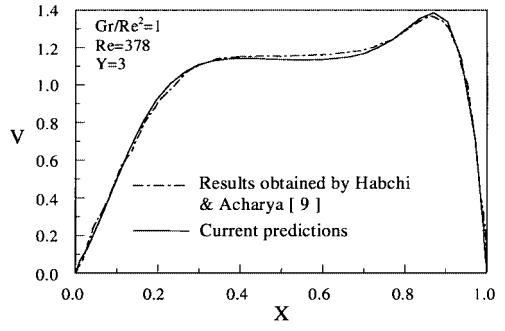

Fig. 3a Velocity distributions across a straight channel heated from one side.

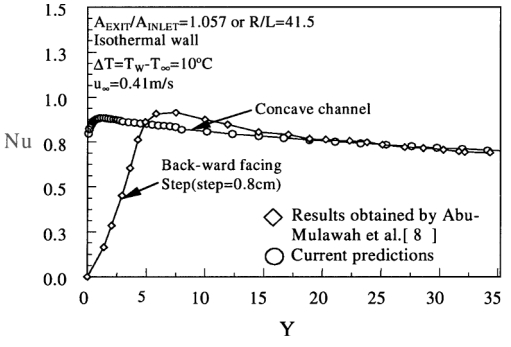

Fig. 3b Comparison of local Nusselt-number distributions in a concave channel with that in a channel with a backstep.

Streamlines and Isotherms

Streamline plots are presented in Fig. 4 for different values of Gr/Re^2 and two different values of R/L (1.04 and 2.5). As shown in Figs. 4a–4d, for the case where $R/L = 1.04$, i.e., when the concave channel is nearly a quarter of a circle, and for $Gr/Re^2 = 0$ and 0.1, a recirculation zone is formed at the exit of the concave section of the channel and is located along the heated surface. This separation of the flow is caused by the expansion of the channel and the adverse pressure gradient associated with it. As Gr/Re^2 increases, the near hot-wall fluid is accelerated by buoyancy forces resulting in a decrease in the size of the recirculation zone. For a critical value of Gr/Re^2, buoyancy forces near the hot surface come into equilibrium with pressure and viscous forces causing separation to

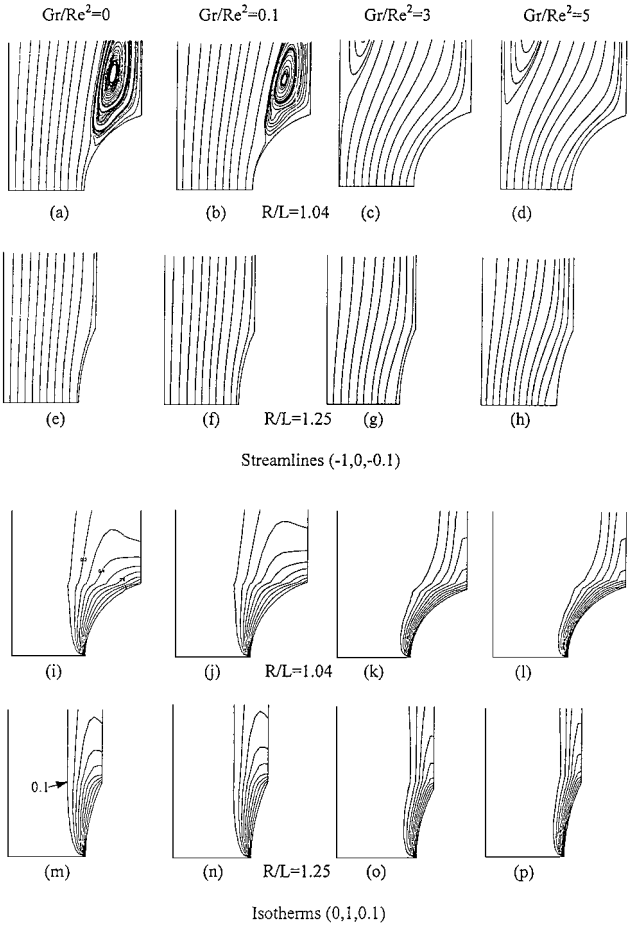

Fig. 4 Streamline and isotherm plots for concave channels.

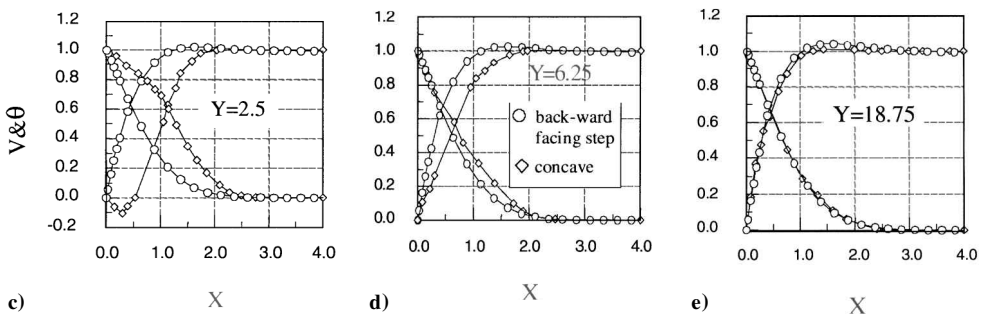

Figs. 3c–3e Comparison of velocity and temperature distributions in a concave channel with that in a channel with a backstep.

disappear. Increasing Gr/Re^2 beyond that value, buoyancy forces overwhelm pressure and viscous forces, thus increasing the velocity of the near hot-wall fluid further. Because the mass-flow rate at any streamwise location is constant, the velocity away from the hot wall decreases. Therefore, the velocity near the adiabatic wall decreases until its value comes close to zero, causing separation of the flow to occur there. The size of this separation bubble, according to the preceding discussion, should increase as Gr/Re^2 increases, which is shown in Figs. 4c and 4d. As the concavity of the channel is decreased (i.e., as R/L is increased), the degree of channel's expansion is reduced, which, in turn, reduces the deceleration of the fluid and causes the size of the separation bubble to diminish until it vanishes for a certain value of R/L and Gr/Re^2. Figures 4e–4h indicate that at $R/L = 2.5$ no separation is encountered over the Gr/Re^2 ranges studied.

The corresponding isotherm plots presented in Fig. 4 reflect the just-described behavior. At low values of Gr/Re^2, caused by the recirculation zone near the exit of the heated concave section of the channel, the temperature gradients are relatively small. As Gr/Re^2 increases and the recirculation bubble disappears along the heated wall, a stronger thermal plume, characterizing boundary-layer type flows, rises along the heated wall and is evident from the concentration of isotherms in the hot-wall region. A similar behavior is observed for higher values of R/L (Figs. 4m–4p), where separation along the heated wall is not encountered and the isotherms reflect a thermal boundary-layer-type behavior along the heated wall.

Temperature and Velocity Distributions

The effects of buoyancy forces on temperature and velocity profiles are displayed in Figs. 5 and 6, respectively. In Fig. 5a the temperature distributions across the midheight of the channel are presented for an aspect ratio of 1.04. As shown, temperature profiles exhibit a boundary-layer behavior with steeper gradients at higher values of Gr/Re^2, indicating higher heat-transfer rates. At higher Gr/Re^2 values natural convection becomes increasingly more important and, hence, accelerates the flow along the curved hot wall resulting in an increase in convection heat-transfer coefficient. In the present concave-channel situation, while buoyancy accelerates the flow in the streamwise direction, the increase in the channel cross-sectional area in the streamwise direction causes flow deceleration.

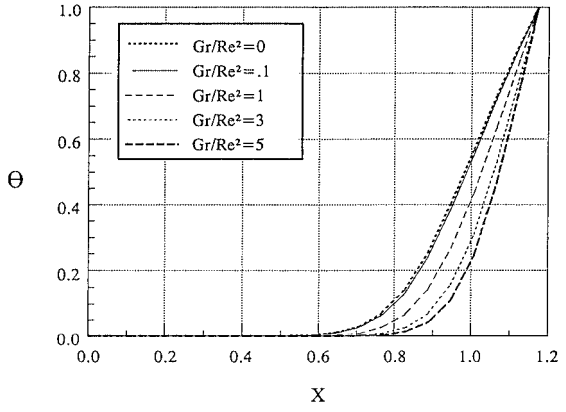

Fig. 5a Temperature distributions across the midheight of the concave channel (*R/L* = 1.04).

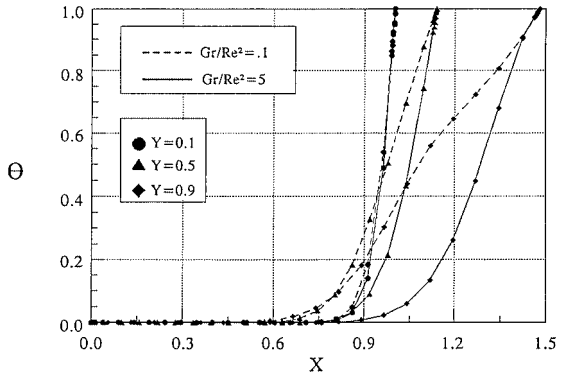

Fig. 5b Temperature distributions at three streamwise locations of the concave channel (*R/L* = 1.25).

The temperature profiles at three different cross-stream locations along the channel ($Y = 0.1, 0.5, 0.9$), for the case when $R/L = 1.25$ and for Gr/Re^2 of 0.1 and 5, are depicted in Fig. 5b. These profiles expectedly indicate steeper gradients and thinner thermal boundary layers near the inlet of the channel. The profiles for both Gr/Re^2 close to the channel inlet ($Y = 0.1$) are nearly identical because buoyancy is not strongly established at this location. As the flow proceeds downstream, buoyancy effects manifest themselves, and the curves for different Gr/Re^2 values are seen to be further apart.

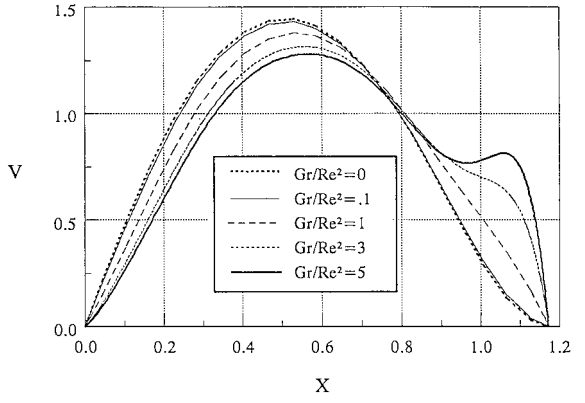

Fig. 6a Velocity distributions across the midheight of the concave channel (*R/L* = 1.04).

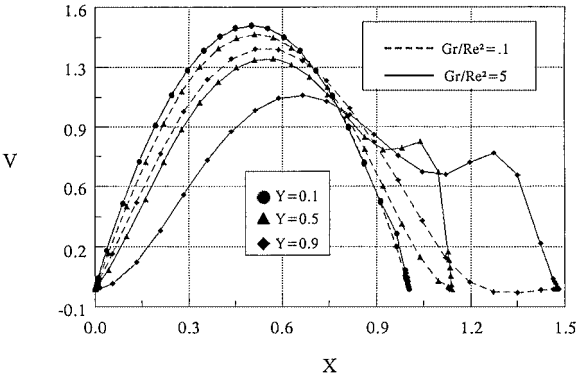

Fig. 6b Velocity distributions at three streamwise locations of the concave channel (*R/L* = 1.25).

The plots displayed in Fig. 6a reveal that the velocity profile across the midheight of the channel at low Gr/Re^2 value ($Gr/Re^2 = 0$ and 0.1) has almost a parabolic distribution and is nearly symmetrical. As Gr/Re^2 increases, the profiles peak near the heated wall because of the increase in buoyancy forces, which accelerate the fluid along the hot wall. Flow acceleration along the heated wall is associated with flow deceleration at other cross-stream locations to ensure mass conservation. Therefore, as Gr/Re^2 increases, the velocity profiles peak near the heated wall, but the maximum velocity of the fluid decreases with the location of the maximum moving towards the hot wall. At constant Gr/Re^2 (Fig. 6b) the maximum velocity in the channel decreases as the flow proceeds downstream because of the increase in the channel's cross-sectional area. The velocity profile near the inlet ($Y = 0.1$) is more or less unaffected by Gr/Re^2; this was also observed in the temperature plots of Fig. 5. Further downstream, the influence of Gr/Re^2 is much higher, with the higher buoyancy forces accelerating the flow adjacent to the hot wall and creating a local peak.

Table 2 Average Nusselt number values in concave and convex channels

	1.04[a] (1.35, 35%)[b]			1.25 (1.159, 15.9%)			2.5 (1.029, 2.9%)			∞ (1, 0%)	∞ (1.029, 2.9%)	∞ (1.159, 15.9%)	∞ (1.35, 35%)
Gr/Re^2	$\overline{Nu}$	$\%\Delta Nu_h$	$\%\Delta Nu_l$	$\overline{Nu}$	$\%\Delta Nu_h$	$\%\Delta Nu_l$	$\overline{Nu}$	$\%\Delta Nu_h$	$\%\Delta Nu_l$	$\overline{Nu}$	$\overline{Nu}$	$\overline{Nu}$	$\overline{Nu}$
Concave channels													
0	8.25	−0.96	−12.51	7.82	−6.12	−10.53	7.86	−5.64	−6.87	8.33	8.44	8.74	9.43
0.1	8.32	−0.83	−12.05	7.85	−6.44	−11.40	7.93	−5.48	−6.71	8.39	8.50	8.86	9.46
1	9.17	3.85	−9.30	8.52	−3.51	−9.36	8.50	−3.74	−5.24	8.83	8.97	9.40	10.11
3	10.57	10.10	−5.29	9.68	0.83	−6.02	9.45	−1.56	−3.18	9.60	9.76	10.30	11.16
5	11.48	12.77	−3.77	10.48	2.95	−4.38	10.13	−0.49	−2.22	10.18	10.36	10.96	11.93
Convex channels													
0	10.35	24.25	9.76	9.26	11.16	5.95	8.55	2.64	1.30	8.33	8.44	8.74	9.43
0.1	10.48	24.91	10.78	9.31	10.97	5.08	8.61	2.62	1.29	8.39	8.50	8.86	9.46
1	10.88	23.22	7.62	9.69	9.74	3.09	9.03	2.26	0.67	8.83	8.97	9.40	10.11
3	11.68	21.67	4.66	10.42	8.54	1.17	9.76	1.67	0.00	9.60	9.76	10.30	11.16
5	12.34	21.22	3.44	11.02	8.25	0.55	10.33	1.47	−0.29	10.18	10.36	10.96	11.93

[a] R/L. [b] $(S, \%\Delta S)$.

Local and Average Nusselt Numbers

The heat-transfer effectiveness of the channel is displayed in terms of local and average Nusselt-number values. The local heat-transfer coefficient and Nusselt number are calculated along the heated wall using the following equations:

$$Nu_S = hS/k \tag{10}$$

$$h = -k\left(\frac{\mathrm{d}T}{\mathrm{d}n}\right)_{\text{wall}} \Big/ (T_w - T_0) \tag{11}$$

where S is the total length of the heated section and n is the normal distance to the wall.

The effects of varying Gr/Re^2 on local Nusselt number Nu_S variation along the hot wall are illustrated in Fig. 7a for the two cases of $R/L = 1.25$ and ∞ where there is no flow separation at any Gr/Re^2. The Nusselt-number profiles for both cases therefore look similar with a peak at the inlet followed by a subsequent streamwise decay along the heated surface as the near-wall fluid becomes hotter. In general, the level of Nu_S increases as the buoyancy forces increase because of the acceleration of the near-wall fluid by buoyancy. For the curved channel at $R/L = 1.25$, the effects of the added surface area (which increases buoyancy-induced acceleration and heat transfer) is partially offset by the increasing cross-sectional area (which decreases the velocity and surface heat transfer).

The effects of changing R/L on the distribution of Nusselt number along the hot wall is depicted in Fig. 7b. The $Gr/Re^2 = 1$ case is selected for presentation because no significant separation is noted along the heated wall, and therefore Nu_S variations for the different R/L cases considered are a consequence primarily of the heated surface area and changes in the flow cross-sectional area. As shown, decreasing R/L increases the heat-transfer surface area, which in turn increases the overall heat transfer with the highest increase being associated with the lowest aspect ratio ($R/L = 1.04$). On the other hand, the cross-sectional area increases by the greatest extent for the smallest aspect ratio (R/L) case, and this case is therefore associated with the most adverse pressure gradient and flow deceleration. Therefore, as R/L decreases, because of the counteracting effects of added heat-transfer surface area and increasing cross-sectional area, the Nusselt-number profiles do not show significant differences with respect to each other. The effect of the added heat-transfer area is slightly greater than the opposing effect of the adverse pressure gradient, and when the local Nusselt number profiles are integrated, the average Nusselt number (presented next) increases with decreasing R/L.

Average Nusselt numbers over the hot surface are calculated using the following equation:

$$\overline{Nu} = \frac{1}{S}\int_S Nu_S \,\mathrm{d}S \tag{12}$$

and tabulated in Table 2 for $R/L = 1.04$, 1.25, 2.5, and ∞. Computed values are compared with corresponding estimates obtained in straight channels. The first comparison is made with straight channels of heights equal to those of the concave channels and consequently with heated areas smaller than those of the concave channels. The second comparison is with straight channels of heated areas equal to those of concave channels, and these channels are consequently taller. The comparison is quantitatively shown in Table 2, where $\%\Delta Nu_h$ and $\%\Delta Nu_l$ represent the percent increase or decrease in heat transfer in a concave channel as compared to a straight channel of equal height or equal heated length, respectively. Moreover, S and $\%\Delta S$ displayed in Table 2 represent the length and the percent increase in length of the heated section as compared to a straight channel of equal height. In all cases (Table 2) $\overline{Nu}$ increases with increasing Gr/Re^2 and/or decreasing R/L, which is expected because increasing Gr/Re^2 accelerates the near hot-wall fluid, as explained earlier, and decreasing R/L increases the heat-transfer surface area.

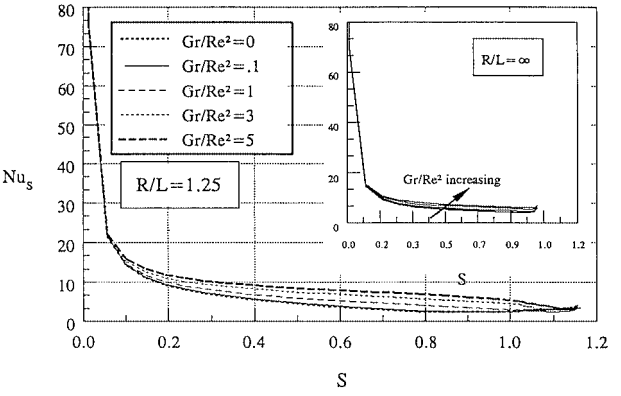

Fig. 7a Effect of buoyancy on local Nusselt-number distributions along the hot wall of the concave channel ($R/L = 1.25$ and ∞).

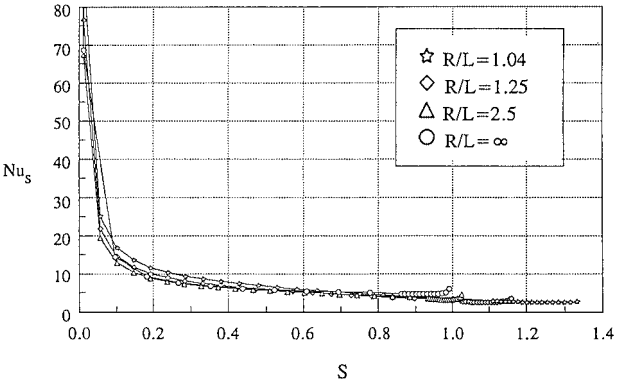

Fig. 7b Effect of channel aspect ratio on local Nusselt-number distribution along the hot wall of the concave channel ($Gr/Re^2 = 1$).

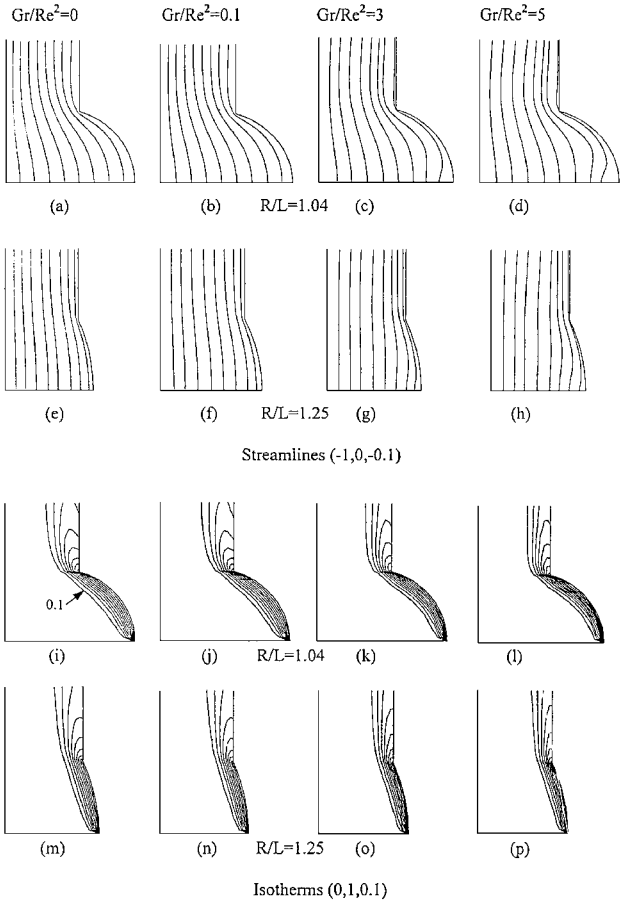

Fig. 8 Streamline and isotherm plots for convex channels.

Comparing channels of equal heights, the results indicate that at low Gr/Re^2 the heat transfer from concave channels is lower than its counterpart in straight channels because of the decrease in surface heat transfer caused by the recirculation resulting from the divergence in the channel. This separation-induced decrease in Nu_S exceeds the increase in the surface heat transfer associated with the greater heated surface area of the concave channel. This is true at all aspects ratios. At high Gr/Re^2 values, however, concave channels of low R/L have higher heat-transfer rates caused by the absence of separation combined with the buoyancy acting over a longer distance along the hot wall. It can be inferred from Table 2 that at a given Gr/Re^2 there exist critical R/L for which the total heat transfer is minimum. The value of this critical aspect ratio is seen to increase with increasing Gr/Re^2.

Comparing channels of equal heated lengths, results show $\overline{Nu}$ to be consistently lower in the concave channel. Because now the comparison is based on equal heated surface areas, the differences in heat transfer for the different cases are directly attributable to the velocities adjacent to the heated surface in the channel. For concave channels because of the larger flow cross-sectional area, the velocities are lower. The differences ($\% \ \Delta Nu_L$) decrease with increasing Gr/Re^2 presumably because the flow remains attached on the curved surface at higher values of Gr/Re^2 as it does in a straight channel, and geometrical effects are weak. The differences also decrease with increasing R/L because the concavity decreases and the geometry increasingly approaches the straight channel geometry.

The average Nusselt-number values displayed in the upper half of Table 2 along with the estimates for $R/L = 5$ and 10, which are not displayed for compactness, are correlated with a maximum deviation of less than $\pm 7.03\%$ via the following relation:

$$\overline{Nu} = 8.1[1 + 1/(R/L)]^{0.035}(1 + Gr/Re^2)^{0.141} \qquad (13)$$

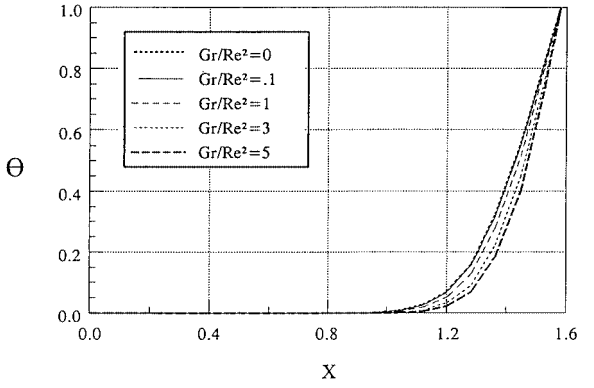

Fig. 9a Temperature distributions across the midheight of the convex channel ($R/L = 1.04$).

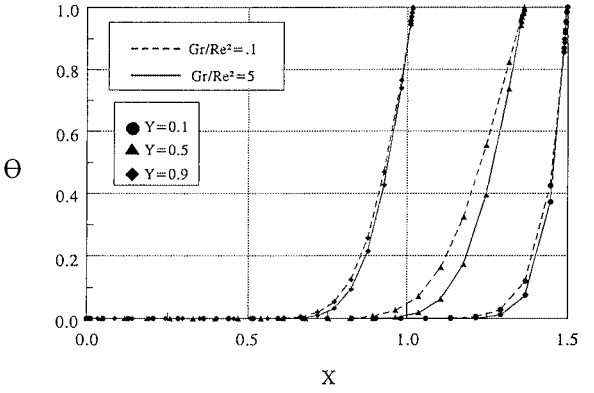

Fig. 9b Temperature distributions at three streamwise locations of the convex channel ($R/L = 1.25$).

Convex Channels

In convex channels the surface curvature increases the heated surface area and decreases the flow cross section in the streamwise direction. These effects aid each other and contribute to an increase in the overall surface heat transfer.

Streamlines and Isotherms

The effects of Gr/Re^2 on the flow and temperature fields are presented in Fig. 8. As shown, streamlines follow the shape of the channel. Moreover, there is no recirculation associated with the convex channel because of its convergence that increases the velocity and decreases the pressure. In view of the absence of separation, the convex channel is likely to have higher heat-transfer rates than the concave channels. Further, isotherms are more concentrated near the hot wall indicating a boundary-layer-type behavior. This clustering of isotherms, which is higher at higher Gr/Re^2, may be explained by noting that increasing the buoyancy forces increases the near hot-wall fluid velocity and thereby the heat-transfer coefficient. Higher heat-transfer coefficients are associated with higher temperature gradients, and consequently the isotherms show denser clustering at higher Gr/Re^2 values.

Temperature and Velocity Distributions

The temperature and velocity profiles at several cross-stream locations along the channel and for different values of Gr/Re^2 are displayed in Figs. 9 and 10, respectively. The effects of buoyancy on temperature (Fig. 9a) and velocity (Fig. 10a) profiles across the midheight of a channel of $R/L = 1.04$ are seen to be similar to those obtained in a concave channel. The primary difference is that the velocity and temperature gradients near the heated wall are stronger for the convex channel because of the combined effects of buoyancy and flow acceleration caused by the decreasing cross-sectional area. Recall that in the concave channel buoyancy accelerated the flow while the increasing cross-sectional area decelerated the flow.

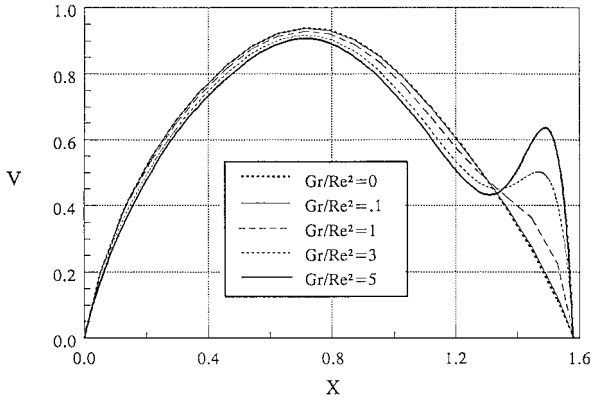

Fig. 10a Velocity distributions across the midheight of the convex channel ($R/L = 1.04$).

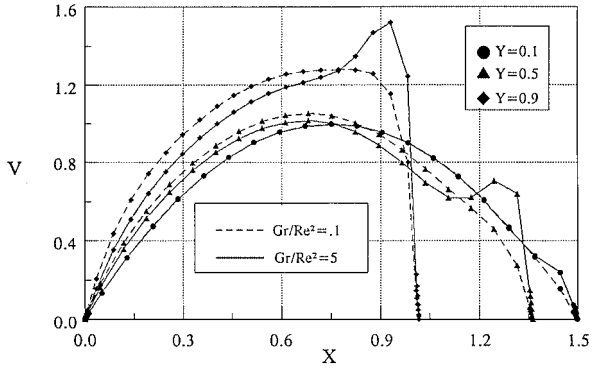

Fig. 10b Velocity distributions at three streamwise locations of the convex channel ($R/L = 1.25$).

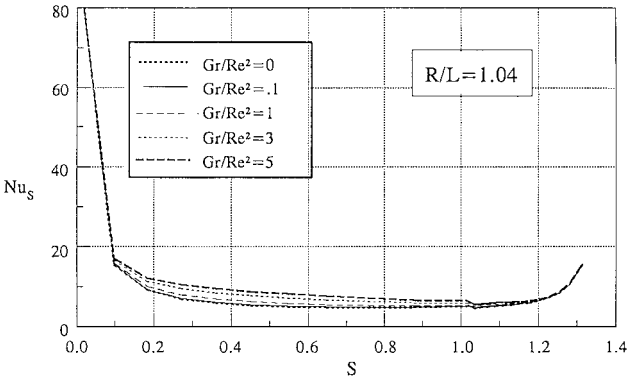

Fig. 11a Effects of buoyancy forces on local Nusselt-number distributions along the hot wall ($R/L = 1.04$).

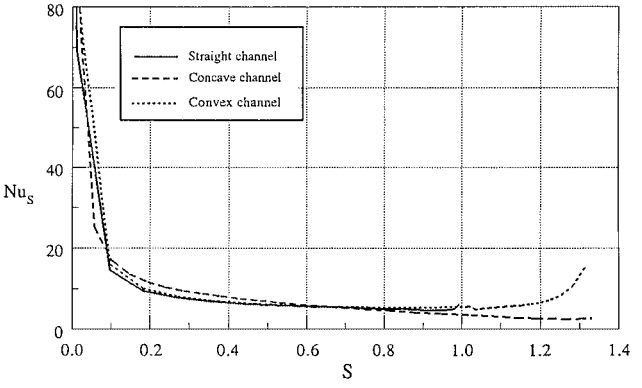

Fig. 11b Comparison of local Nusselt-number distributions along the hot wall of a concave and convex channel ($R/L = 1.04$) with the Nusselt number for a straight vertical channel of equal height ($Gr/Re^2 = 1$).

The temperature and velocity profiles at several locations along the channel are presented in Figs. 9b and 10b, respectively. In both figures profiles are displayed at three different locations ($Y = 0.1$, 0.5, and 0.9) along a channel of an aspect ratio 1.25 and for two Gr/Re^2 values ($Gr/Re^2 = 0.1$ and 5). An observation to be made in Fig. 9b is that as the flow proceeds downstream the influence of Gr/Re^2 increases initially (at $Y = 0.5$) because of buoyancy-induced acceleration, and then becomes less distinctive (at $Y = 0.9$) because of flow acceleration associated with area reduction in the concave channel. Therefore, the forced-convection effects become dominant near the exit of the channel. Thus, the use of convex channels increases the relative importance of forced-convection heat transfer.

The velocity profiles (Fig. 10b) reveal that at constant Gr/Re^2 the maximum velocity in the channel increases as the flow proceeds downstream because of the decrease in the channel's cross-sectional area and the effect of buoyancy. At $Gr/Re^2 = 0.1$ buoyancy effects are weak, and the increase in the channel velocities is caused primarily by decreasing flow cross-sectional area. At $Gr/Re^2 = 5$ buoyancy effects are strong, and the differences in this profile compared to the $Gr/Re^2 = 0.1$ profile are directly caused by the additional buoyancy effects. These buoyancy-induced differences are primarily confined to the region near the heated wall. Note that the concave-channel profiles at high and low Gr/Re^2 values show much greater disparity than the convex channel profiles because of the opposing effects of buoyancy and increasing cross section in the concave channel and the aiding effects of buoyancy and decreasing cross section in a convex channel.

Local and Average Nusselt Numbers

The local heat-transfer coefficient and Nusselt number along the hot wall are calculated using Eq. (11). The local Nusselt-number Nu_S distribution for various values of Gr/Re^2 is presented in Fig. 11a. As stated earlier, the maximum value of the local Nusselt number occurs at the inlet of the channel. As the fluid proceeds downstream, its temperature rises, and, consequently, the corresponding local Nusselt number decreases. As the flow approaches the exit of the convex section, Nu_S shows a further increase, which is because of the acceleration of the fluid toward the exit of the channel. Such behavior increases the overall heat transfer in convex channels as compared to concave and straight channels.

Figure 11b gives a clearer view of the effects of the channel's configuration on the distribution of Nu_S. In the entrance region ($S < 0.05$) the convex channel has the highest heat transfer; in the midspan regions ($0.05 < S < 1$) the differences are rather small with the concave channel having the highest Nu_S values and the straight channel having the lowest values. As the flow proceeds downstream, the picture changes, and the convex channel achieves the highest and the concave channel the lowest values of Nu_S because of their converging and diverging shapes, respectively. The differences in this region ($S > 1$) are quite significant, with Nusselt numbers varying by a factor of 2–4.

The overall heat transfer results [$\overline{Nu}$, Eq. (12)] in convex channels are compared with corresponding values obtained in straight channels (Table 2). For all cases $\overline{Nu}$ increases with increasing Gr/Re^2 caused by buoyancy-induced acceleration and/or decreasing R/L caused by acceleration induced by a reduction in the cross-sectional area. Moreover, results reveal that convex channels enhance heat transfer significantly more as compared to concave channels. This, as noted earlier, is because buoyancy and cross-sectional area changes aid each other in convex-channel flows and oppose each other in concave-channel flows. As expected, increasing the aspect ratio R/L decreases the percent increase caused by the decrease in the available heat-transfer area. A maximum increase of 24.9% is achieved by the channel of the lowest aspect ratio ($R/L = 1.04$) and at the lowest value of buoyancy ($Gr/Re^2 = 0.1$). Table 2 also shows that convex channels still provide higher values of $\overline{Nu}$ even when compared with those obtained over longer straight channels of equal heated length.

The average Nusselt number values, displayed in the lower half of Table 2 along with values obtained for $R/L = 5$ and 10, are correlated as

$$\overline{Nu} = 8.08[1 + 1/(R/L)]^{0.271}(1 + Gr/Re^2)^{0.103} \qquad (14)$$

with a maximum deviation of less than $\pm 6.32\%$.

Conclusion

A numerical study of laminar mixed-convection heat transfer in concave and convex channels was presented. Results indicated that convex channels provide significant improvements in heat transfer over straight channels of equal heights or equal heated lengths. The rate of this heat-transfer enhancement was found to increase with decreasing aspect ratio and increasing buoyancy forces. In concave channels the heat-transfer rate was found to increase relative to straight channels of equal heights only at high values of Gr/Re^2. Compared to straight channels of equal heated lengths, the heat-transfer rate in a concave channel is always found to decrease.

Acknowledgment

The financial support provided by the University Research Board of the American University of Beirut through Grant 113040-48756 is gratefully acknowledged.

References

[1]Ostrach, S., "Combined Natural and Forced Convection Laminar Flow and Heat Transfer of Fluids With and Without Heat Source in Channels with Linearly Varying Wall Temperature," NACA TN 3141,1954.

[2]Tao, L. N., "On Combined Free and Forced Convection in Channels," *Journal of Heat Transfer*, Vol. 82, No. 3, 1960, pp. 233–238.

[3]Lawrence, W. T., and Chato, J. C., "Heat Transfer Effects on the Developing Laminar Flow Inside Vertical Tube," *Journal of Heat Transfer*, Vol. 88, No. 2, 1966, pp. 214–222.

[4]Zeldin, B., and Schmidt, F. W., "Developing Flow with Combined Free-Forced Convection in an Isothermal Vertical Tube," *Journal of Heat Transfer*, Vol. 94, 1972, pp. 211–223.

[5]Habchi, S., and Acharya, S., "Laminar Mixed Convection in a Symmetrically or Asymmetrically Heated Vertical Channel," *Numerical Heat Transfer*, Vol. 9, 1986, pp. 605–616.

[6]Hong, B., Armaly, B. F., and Chen, T. S., "Laminar Mixed Convection in a Duct with a Backward-Facing Step—The Effects of Inclination Angle and Prandtl Number," *International Journal of Heat and Mass Transfer*, Vol. 36, 1993, pp. 3059–3067.

[7]Abu-Mulaweh, H. I., Aramaly, B. F., and Chen, T. S., "Measurements in Buoyancy-Opposing Laminar Flow over a Vertical Backward-Facing Step," *Journal of Heat Transfer*, Vol. 116, No. 1, 1994, pp. 247–250.

[8]Abu-Mulaweh, H. I., Aramaly, B. F., and Chen, T. S., "Effects of Upstream Wall Heating on Mixed Convection in Separated Flows," *Journal of Thermophysics and Heat Transfer*, Vol. 9, No. 4, 1995, pp. 715–721.

[9]Habchi, S., and Acharya, S., "Laminar Mixed Convection in a Partially Blocked, Vertical Channel," *International Journal of Heat and Mass Transfer*, Vol. 29, No. 11, 1986, pp. 1711–1722.

[10]Moukalled, F., and Acharya, S., "Forced Convection Heat Transfer in a Finitely Conduction Externally Finned Pipe," *Journal of Heat Transfer*, Vol. 110, No. 3, 1988, pp. 571–576.

[11]Moukalled, F., Darwish, M., and Acharya, S., "Laminar Mixed Convection Heat Transfer in Externally Finned Pipes," *Journal of Enhanced Heat Transfer*, Vol. 3, No. 1, 1996, pp. 29–42.

[12]Moukalled, F., Darwish, M., and Acharya, S., "Influence of Wall Conduction on Mixed Convection Heat Transfer in Externally Finned Pipes," *Numerical Heat Transfer*, Pt. A, Vol. 28, No. 2, 1995, pp. 157–173.

[13]Moukalled, F., Kassamani, J., and Acharya, S., "Turbulent Convection Heat Transfer in Longitudinally Conduction, Externally Finned Pipes," *Numerical Heat Transfer*, Pt. A, Vol. 21, 1992, pp. 401–421.

[14]Agonafer, D., and Watkins, C. B., "Numerical Solution of Natural Convection Between Diverging Plates," American Society of Mechanical Engineers, Winter Annual Meeting, Nov. 1984.

[15]Kestoras, M. D., and Simon, T. W., "Hydrodynamic and Thermal Measurements in a Turbulent Boundary Layer Recovering from a Concave Curvature," *Journal of Turbomachinery*, Vol. 114, No. 4, 1992, pp. 891–898.

[16]Finnis, M. V., and Brown, A., "The Streamwise Development of Gortler Vortices in a Favorable Pressure Gradient," *Journal of Turbomachinery*, Vol. 118, 1996, pp. 162–171.

[17]Patankar, S. V., *Numerical Heat Transfer and Fluid Flow*, Hemisphere, New York, 1980, pp. 52–54, 126–131.

[18]Peric, M., "A Finite Volume Method for the Prediction of Three-Dimensional Fluid Flow in Complex Ducts," Ph.D. Dissertation, Imperial College of Science and Technology, Univ. of London, London, 1985.

[19]Thompson, J. F., *Numerical Grid Generation*, North-Holland, Amsterdam, 1982.